University of Kentucky
UKnowledge

Physics and Astronomy Faculty Publications

Physics and Astronomy

$^{12}C/^{13}C$ Ratio in Planetary Nebulae from the *IUE* Archives

R. H. Rubin
NASA Ames Research Center

Gary J. Ferland
University of Kentucky, gary@uky.edu

E. E. Chollet
NASA Ames Research Center

R. Horstmeyer
NASA Ames Research Center

Right click to open a feedback form in a new tab to let us know how this document benefits you.

Follow this and additional works at: https://uknowledge.uky.edu/physastron_facpub

Part of the Astrophysics and Astronomy Commons, and the Physics Commons

^{12}C/^{13}C Ratio in Planetary Nebulae from the *IUE* Archives

Notes/Citation Information

Published in *The Astrophysical Journal*, v. 605, no. 2, p. 784-792.

Digital Object Identifier (DOI)

^{12}C/^{13}C RATIO IN PLANETARY NEBULAE FROM THE *IUE* ARCHIVES

R. H. RUBIN,[1,2] G. J. FERLAND,[3] E. E. CHOLLET,[1] AND R. HORSTMEYER[1]

ABSTRACT

We investigated the abundance ratio of ^{12}C/^{13}C in planetary nebulae by examining emission lines arising from C III $2s2p\ ^3P^o_{2,1,0} \rightarrow 2s^2\ ^1S_0$. Spectra were retrieved from the *International Ultraviolet Explorer* archives, and multiple spectra of the same object were co-added to achieve improved signal-to-noise ratio. The ^{13}C hyperfine structure line at 1909.6 Å was detected in NGC 2440. The ^{12}C/^{13}C ratio was found to be $\sim 4.4 \pm 1.2$. In all other objects, we provide an upper limit for the flux of the 1910 Å line. For 23 of these sources, a lower limit for the ^{12}C/^{13}C ratio was established. The impact on our current understanding of stellar evolution is discussed. The resulting high–signal-to-noise ratio C III spectrum helps constrain the atomic physics of the line formation process. Some objects have the measured 1907/1909 Å flux ratio outside the low–electron density theoretical limit for ^{12}C. A mixture of ^{13}C with ^{12}C helps to close the gap somewhat. Nevertheless, some observed 1907/1909 Å flux ratios still appear too high to conform to the currently predicted limits. It is shown that this limit, as well as the 1910/1909 Å flux ratio, are predominantly influenced by using the standard partitioning among the collision strengths for the multiplet $^1S_0 - {}^3P^o_J$ according to the statistical weights. A detailed calculation for the fine-structure collision strengths between these individual levels would be valuable.

Subject headings: atomic processes — ISM: abundances — planetary nebulae: general — planetary nebulae: individual (NGC 2440) — stars: abundances — stars: AGB and post-AGB

1. INTRODUCTION

The relative abundances of ^{12}C and ^{13}C in evolved stars present a strong challenge to our current understanding of stellar nucleosynthesis. A growing body of observational evidence suggests that standard stellar models greatly overestimate the ratio of ^{12}C to ^{13}C on the red giant branch (RGB) and later evolution. In a careful study of the literature, Charbonnel & do Nascimento (1998) have shown that a full 96% of evolved stars exhibit a ^{12}C/^{13}C ratio below 15, considerably lower than models predict (^{12}C/^{13}C between 20 and 30). On the other hand, cool-bottom processing (CBP), which employs a deep mixing mechanism below the standard convective envelope during the red giant phase (Sackmann & Boothroyd 1999), predicts ^{12}C/^{13}C ratios ≤ 20 for low-mass post-RGB stars (Boothroyd & Sackmann 1999). Using millimeter wave observations of ^{12}CO and ^{13}CO, Palla et al. (2000) found several examples of planetary nebulae (PNs) with small ^{12}C/^{13}C ratios, as low as 9 for NGC 7293. Balser, McMullen, & Wilson (2002) in a similar study measured ^{12}CO and ^{13}CO in molecular clouds associated with PNs. They found the range of ^{12}C/^{13}C from 2.2 to 31 in nine PNs. The lowest value 2.2 ± 0.03 was found for the PN M1-16. Developing another approach to obtaining these abundance ratios is very valuable for corroborating these low values.

Clegg (1985) pointed out that the ^{12}C/^{13}C ratio could be determined using an extremely weak C III ^{13}C line at 1909.597 Å. This line is a hyperfine induced transition that arises from $2s2p\ ^3P^o_0 \rightarrow 2s^2\ ^1S_0$, which is strictly forbidden in ^{12}C. By comparing the flux of this line to the nearby bright C III lines $2s2p\ ^3P^o_{2,1} \rightarrow 2s^2\ ^1S_0$ at 1906.683 and 1908.734 Å,

respectively, one can find the ^{12}C/^{13}C ratio. Using the *Hubble Space Telescope* (*HST*), Clegg et al. (1997) found a ratio of 15 ± 3 in NGC 3918 and 21 ± 11 in SMC N2, as well as a very marginal 7^{+14}_{-3} for LMC N122. Palla et al. (2002), also using *HST*, reported a nondetection in NGC 3242, showing ^{12}C/^{13}C ≥ 38.

When studying faint lines in extended sources, the light-gathering power of the instrument is extremely important. The large *International Ultraviolet Explorer* (*IUE*) aperture, an $\sim 20'' \times \sim 10''$ rounded rectangle (also described as an oval or race-track pattern), allowed a high throughput for extended objects like PNs. The extensive archival database and New Spectral Image Processing System (NEWSIPS) allow us to effectively study the 1909.597 Å ^{13}C line with *IUE*. Using these data, co-adding multiple spectra when available to get a higher signal-to-noise ratio (S/N), we attempt to measure or provide upper limits for the flux of this line. In conjunction with our measurements of fluxes in the adjacent "main" lines, we derive or set limits for the ^{12}C/^{13}C ratio in most of the sample of PNs.

In § 2, we discuss the *IUE* database and our flux measurements. The analysis tools for interpreting the observations are introduced in § 3, with the population rate equations. In § 4, the flux ratios are analyzed in terms of the ^{12}C/^{13}C ratio and the electron density (N_e). Section 5 contains a discussion and conclusions.

2. *IUE* OBSERVATIONS

The data were obtained from the *IUE* archives. For most sources, only short-wavelength prime (SWP) camera spectra with the large aperture were used, because the long-wavelength spectra taken with both the prime camera (LWP) and redundant camera (LWR) are much noisier at this wavelength. The spectral resolution of high-dispersion SWP, LWP, or LWR spectra at these wavelengths is ~ 0.2 Å, sufficient to separate the weak ^{13}C line from the bright line at 1908.7 Å.

[1] NASA Ames Research Center, Moffett Field, CA 94035-1000; rubin@cygnus.arc.nasa.gov.

[2] Orion Enterprises, M.S. 245-6, Moffett Field, CA 94035-1000.

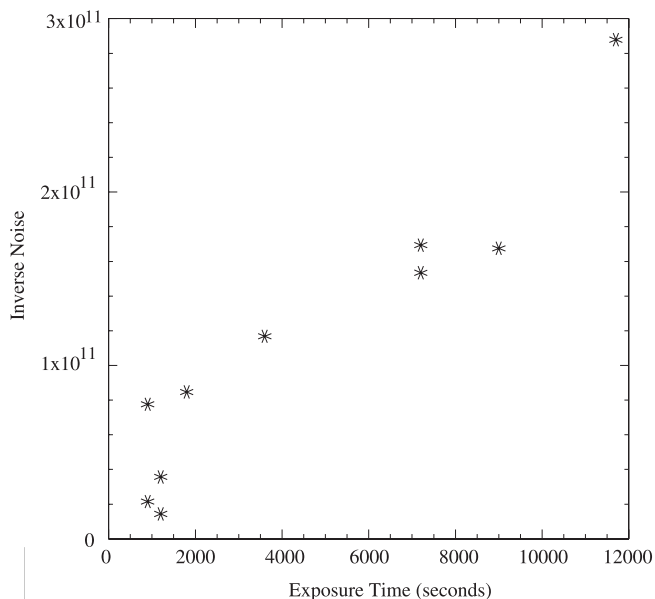[3] University of Kentucky, Department of Physics and Astronomy, Lexington, KY 40506; gary@pa.uky.edu.

Fig. 1.—Inverse noise (the reciprocal of the sum of noise points from ∼1910.5–1920 Å) versus the exposure time for the various SWP high-dispersion, large-aperture *IUE* spectra of NGC 3918. Units in the ordinate are relative; a larger value indicates less noisy data.

We included all promising PNs observed with high dispersion in the large aperture. Multiple observations of the same object were co-added point by point, weighted by the inverse of the total noise in the continuum, to improve the S/N, using our own analysis program. We note that the inverse noise and exposure time are not linearly related in *IUE* spectra. Figure 1 shows a plot of inverse noise versus integration time for NGC 3918 SWP spectra. Though the data quality, as gauged by inverse noise, generally improves with increased time, the quality is not a linear relation of either exposure time or the square root of the exposure time. The *IUE* on-line Frequently Asked Questions[4] recommends inverse noise weighting, and our data show that weighting by the inverse noise generates better S/N than weighting by the time or by the square root of the time.

The ISAP[5] routine *line fit* was used to fit a three-component Gaussian to the three lines of the C III multiplet in order to determine the line fluxes or to set an upper limit when a line was not detected. The number of free parameters were limited by constraining the full width at half-maximum (FWHM) to be that of the 1907 Å line. Only one degree of freedom in the determination of wavelength was allowed by requiring the fit to conform to the known $\Delta\lambda_{\mathrm{vac}}$ between the transitions—that is an offset of 2.051 and 2.914 Å for the 1909 and 1910 Å lines, respectively, relative to the 1906.683 Å line. We use a quadratic continuum fit to the line-free data. Most of the *IUE* spectra that we found useful are SWP spectra. For fitting the continuum baseline in these, we avoid the data points at wavelengths shorter than the 1907 Å line, where there is an echelle interorder "splice" (at ∼1905.4 Å) and the fluctuations in the continuum intensity become much larger than those on the red side.

We used both Gaussian fitting and direct integration routines to measure the net line flux above the continuum. Because the filled large aperture introduced a spectral impurity into the spectrograph, the line profiles have flatter tops and less extended bases (i.e., are more "trapezoidal") than the Gaussian fits. For this reason and because some of the sources have lines that depart in other ways from Gaussian, we prefer to use the direct integration routines (the *moment* option in ISAP) to measure the line flux. We also confirmed our line flux results using IRAF[6] *splot* with the "e" option for direct integration.

The root mean square (rms) fluctuations in the continuum flux were determined from a region clear of lines and obvious spikes longward of 1910 Å, and the FWHM determined from the 1906.7 Å line. From this, we determine the value 3 σ, which is our threshold for judging whether a flux measurement is a detection or not. This 3 σ value is also used to set upper limits on the flux for the nondetections. The results of our measurements are presented in Table 1. Column (1) has the source name; columns (2) and (3) have the J2000.0 positions; columns (4), (6), and (8) have the line flux measurements $F(1906.7)$, $F(1908.7)$, and $F(1909.6)$ in ergs cm^{-2} s^{-1}. Column (5) has the 1 σ uncertainty associated with each of the line fluxes, while column (7) has 3 times this value in order to judge whether or not the hyperfine line has been detected. The FWHM from the Gaussian fit of the co-added, unsaturated spectra are in column (9). The entries in the remaining columns are quantities derived from these data and are discussed below.

For many of the sources, there is a second line in Table 1 where more *IUE* spectra were co-added with those used to produce the first-line results (with *only unsaturated data*). These added spectra are saturated in either the 1907 or 1909 Å line. Because of the limited dynamic range of *IUE*, long exposures, particularly with the SWP camera, of bright PNs will readily saturate (overexpose) these strong C III lines. However, there is not a saturation issue with the 1910 Å line and adjacent continuum. Using these additional data, we are able to test if there are now any statistically significant detections of the 1910 Å line by comparing $F(1909.6)$ with the 3 σ uncertainty, which is generally smaller than the entry on line 1. Although the resulting fluxes and FWHMs in the main lines are not reliable, we are able to use these lines as a fiducial wavelength indicator only to fit the data in the vicinity of the 1910 Å line with a single Gaussian that has an FWHM assumed to be the same as on line 1. As discussed in § 4.2, the only object with a significant detection of the 1910 Å line is NGC 2440 (indicated by boldface type). Even with the additional data entered on line 2, we found no other significant detections of this line.

3. RATE EQUATIONS FOR THE LEVEL POPULATIONS

In order to interpret the observational data, we solve the C III statistical equilibrium equations for the populations of the four lowest lying energy levels, numbered 1–4. These are $2s^2\,^1S_0$, $2s2p\,^3P_0^o$, $2s2p\,^3P_1^o$, and $2s2p\,^3P_2^o$. For this, the effective collision strengths (Υ values) and transition rates listed in Table 2 are used. Note the important distinction for A_{21} between ^{12}C and ^{13}C. This is the sole quantity that is different and is the crucial factor in providing different results when solving the rate equations for the level populations.

The effective collision strengths for transitions between the $^3P_J^o$ levels are available for electron temperature $T_e = 5000, 10,000, 15,000,$ and $20,000$ K (Keenan, Feibelman, & Berrington 1992). We use these same temperatures in Table 2, adding the recent data for $^1S_0-^3P_J^o$ (Mitnik et al. 2003 and D. Griffin 2003, private communication). Then, following standard procedure, their value is partitioned among the $^3P_J^o$ levels according to the statistical weights.

The results of the solution of the rate equations for ^{12}C and ^{13}C in terms of the pertinent volume emissivity (j value) ratios are given in Figure 2. In this figure, we plot j_{1907}/j_{1909} for both pure ^{12}C and pure ^{13}C, in addition to j_{1910}/j_{1909} for pure ^{13}C. These ratios are shown versus log $(N_e \text{ cm}^{-3})$ for two values of T_e, 10,000 and 15,000 K. This is a typical range for T_e in PNs and demonstrates that there is minimal dependence on T_e.

Besides the graphical representation shown in Figure 2, it is useful to solve the four-level rate equations explicitly in the low-N_e limit in terms of algebraic expressions for the atomic data. As we present here, this provides superior insight when we compare the observed line ratios with theoretical predictions. The expression for the familiar N_e-diagnostic line ratio may be written

$$\frac{I(1907)}{I(1909)} = \frac{N_4 A_{41} \nu_{41}}{N_3 A_{31} \nu_{31}}. \tag{1}$$

Here we need to obtain N_4/N_3. How this was done for the general three-level atom rate equations may be seen from equations (2) and (3) in Rubin (1986). Because we are writing the equations for just the low-N_e limit, when $A_{21} \neq 0$, all the terms arising from levels above ground that contain the square of the density are dropped (i.e., collisional routes out are negligible). In addition, terms with very low A_{ij} may be neglected. Then, in the low-N_e limit when $A_{21} \neq 0$,

$$\frac{I(1907)}{I(1909)} = 1.001 \frac{C_{14} A_{41}}{C_{13} A_{41} + C_{14} A_{43}}, \tag{2}$$

where $C_{ij} = \Upsilon_{ij} \exp(-\chi_{ij}/kT_e)$. The χ terms are the energy level differences and k is the Boltzmann constant. Because $A_{43} \ll A_{41}$,

$$\frac{I(1907)}{I(1909)} = 1.001 \frac{C_{14}}{C_{13}}. \tag{3}$$

When we assume that all $\exp(-\chi_{1j}/kT_e)$ are approximately the same, then

$$\frac{I(1907)}{I(1909)} \sim \frac{\Upsilon_{14}}{\Upsilon_{13}} = \frac{5}{3}, \tag{4}$$

following the ratio of the statistical weights. This is the equation governing the ^{13}C ratio.

In the low-N_e limit when $A_{21} = 0$, the collisional terms arising from level 2 are retained. Thus, in the low-N_e limit when $A_{21} = 0$:

$$\frac{I(1907)}{I(1909)} = 1.001 \frac{C_{12}\Upsilon_{24} + C_{14}(\Upsilon_{23} + \Upsilon_{24} + \Upsilon_{12})}{C_{12}\Upsilon_{23} + C_{13}(\Upsilon_{23} + \Upsilon_{24} + \Upsilon_{12})}. \tag{5}$$

The last Υ_{12} term arises from collisional de-excitation out of level 2 and the symmetry of Υ_{21} and Υ_{12}. Again, when all

$\exp(-\chi_{1j}/kT_e)$ are nearly the same, then

$$\frac{I(1907)}{I(1909)} \sim \frac{\Upsilon_{12}\Upsilon_{24} + \Upsilon_{14}(\Upsilon_{23} + \Upsilon_{24} + \Upsilon_{12})}{\Upsilon_{12}\Upsilon_{23} + \Upsilon_{13}(\Upsilon_{23} + \Upsilon_{24} + \Upsilon_{12})}. \tag{6}$$

This is the equation governing the ^{12}C ratio. We note that the second terms (including the parenthesized values) in the numerator and denominator dominate, and if the first terms were not present, would give the same result 5/3 as the ^{13}C ratio. It is interesting that the two solutions hinge on just A_{21}. Yet it is true that the low-N_e limits for both the ^{12}C and ^{13}C C III ion depend on the collision strengths.

Let us now consider the ratio $I(1910)/I(1909)$ in the low-N_e limit with $A_{21} \neq 0$. This is for the case of pure ^{13}C. The bottom curve in Figure 2 and the behavior at low N_e that we are about to work out *do not* include any contribution from ^{12}C to the main lines. Starting with

$$\frac{I(1910)}{I(1909)} = \frac{N_2 A_{21} \nu_{21}}{N_3 A_{31} \nu_{31}}, \tag{7}$$

we find

$$\frac{I(1910)}{I(1909)} = 0.9995 \frac{C_{12} A_{41} - C_{14} A_{43}}{C_{13} A_{41} + C_{14} A_{43}}. \tag{8}$$

The comments and assumptions that lead from equation (1) to (2) apply here, except that N_2/N_3 is apropos now. Again, when all $\exp(-\chi_{1j}/kT_e)$ are nearly the same, then

$$\frac{I(1910)}{I(1909)} \sim \frac{\Upsilon_{12} A_{41} - \Upsilon_{14} A_{43}}{\Upsilon_{13} A_{41} + \Upsilon_{14} A_{43}}. \tag{9}$$

The second terms in the numerator and denominator are negligible compared with the first terms; by dropping them, one obtains

$$\frac{I(1910)}{I(1909)} \sim \frac{\Upsilon_{12}}{\Upsilon_{13}} = \frac{1}{3}, \tag{10}$$

following the ratio of the statistical weights.

The equations derived in this section agree extremely well with the low-N_e limits shown in Figure 2. The small variations with T_e are also in agreement between the analytical expressions and Figure 2.

4. INTERPRETATION OF THE OBSERVED LINE FLUXES

It is important to realize that the "main" lines 1907 and 1909 are produced by *both* ^{12}C and ^{13}C. Following Brage et al. (1998), we may write an equation for the intrinsic line ratio $I(1910)/I(1909) = I_{21}/I_{31}$ as

$$\frac{I_{21}}{I_{31}} = \frac{\nu_{21}}{\nu_{31}} \frac{n_2 A_{21}}{(rm_3 + n_3) A_{31}}, \tag{11}$$

where r is the ^{12}C/^{13}C abundance ratio, n_2, n_3, and n_4 are the fractional populations for levels 2, 3, and 4 for ^{13}C, and m_3 and m_4 are the fractional populations for levels 3 and 4 for ^{12}C. That is, the sum over n_i, $i = 1$–4, is unity, as is the sum over m_i. Values of n_i and m_i are determined from solving the respective rate equations.

Object	R.A. (J2000.0)	Decl. (J2000.0)	$F(1906.7)$	$1\,\sigma$ error	$F(1908.7)$	$3\,\sigma$	$F(1909.6)$	FWHM	$F(1907)/F(1909)$	N_e (cm^{-3})	$r(^{12}\mathrm{C}/^{13}\mathrm{C})$
PN G108.4−76.1	00 37 16.0	−13 43 00	2.79E−12	3.42E−14	1.93E−12	1.03E−13	−5.24E−14	0.3670	1.45	1580–2120	>3
	...	...	...	2.04E−14	...	6.11E−14	3.00E−14	...	...	...	...
IC 351	03 47 32.9	+35 02 48	1.71E−12	7.91E−14	1.40E−12	2.37E−13	3.81E−14	0.2955	1.22	8360	—
IC 2003	03 56 22.0	+33 52 28	4.97E−12	8.87E−14	3.40E−12	2.66E−13	−1.26E−13	0.4451	1.46	1170–1950	>1.8
	...	...	...	4.63E−14	...	1.39E−13	−6.39E−14	...	...	...	...
NGC 1535...................	04 14 15.9	−12 44 21	7.99E−12	1.06E−13	5.97E−12	3.17E−13	−1.40E−13	0.5714	1.34	4550–5140	>1.9
	...	...	...	6.35E−14	...	1.91E−13	−6.00E−15	...	...	...	...
IC 418	05 27 28.2	−12 41 50	1.59E−11	9.57E−14	1.42E−11	2.87E−13	1.61E−13	0.3658	1.12	12,300–12,600	>3.4
	...	...	...	4.06E−14	...	1.22E−13	2.70E−14	...	...	...	...
NGC 2022...................	05 42 06.2	+09 05 10	3.56E−12	6.09E−14	2.40E−12	1.83E−13	−5.99E−14	0.6721	1.48	660–1400	>2.1
IC 2149	05 56 24.0	+46 06 15	2.96E−12	3.69E−14	2.26E−12	1.11E−13	2.12E−14	0.3213	1.31	5400–5960	>1.9
	...	...	...	2.80E−14	...	8.39E−14	−5.52E−15	...	...	...	...
IC 2165	06 21 42.6	−12 59 10	1.04E−11	2.05E−13	5.80E−12	6.14E−13	−9.74E−14	0.4423	1.79	out of range	...
	...	...	...	4.73E−14	...	1.42E−13	−6.95E−14	...	...	...	...
NGC 2346...................	07 09 22.5	−00 48 24	7.01E−13	3.29E−14	4.95E−13	9.87E−14	2.66E−14	0.4853	1.42	2360	—
	...	...	...	3.42E−14	...	1.02E−13	1.67E−14	...	...	...	...
NGC 2440	07 41 55.4	−18 12 33	2.24E−11	1.47E−13	1.57E−11	4.41E−13	5.94E−13	0.5399	1.427	2460	**4.4 ± 1.2**
PN G264.4−12.7	07 47 20.4	−51 15 05	7.94E−13	1.92E−14	6.15E−13	5.76E−14	3.01E−14	0.2851	1.29	6000–7080	>0.43
IC 2448	09 07 06.6	−69 56 29	8.06E−12	1.29E−13	5.00E−12	3.87E−13	−1.06E−13	0.3831	1.61	out of range	...
	...	...	...	3.10E−14	...	9.30E−14	5.33E−14	...	...	...	...
NGC 2867...................	09 21 25.5	−58 18 35	2.42E−11	1.26E−13	1.87E−11	3.77E−13	9.22E−14	0.4567	1.29	5900–6130	>5.9
	...	...	...	9.29E−14	...	2.79E−13	4.31E−14	...	...	...	...
NGC 3132...................	10 07 01.8	−40 26 11	1.71E−12	5.43E−13	1.08E−12	1.63E−12	−1.33E−13	0.6262	1.58	out of range	...
	...	...	...	2.21E−13	...	6.63E−13	−1.24E−13	...	...	...	...
NGC 3211...................	10 17 50.4	−62 40 12	7.94E−12	7.74E−14	6.04E−12	2.32E−13	2.24E−14	0.4637	1.31	5250–5680	>2.8
NGC 3242...................	10 24 46.1	−18 38 33	4.71E−11	2.51E−13	3.15E−11	5.31E−13	5.13E−14	0.5662	1.50	370–530	>14.5
	...	...	...	1.00E−13	...	3.00E−13	1.28E−13	...	...	...	...
NGC 3918...................	11 50 17.2	−57 10 53	6.94E−11	2.16E−13	5.48E−11	6.48E−13	1.64E−13	0.4605	1.27	6810–6950	>9.9
	...	...	...	7.69E−14	...	2.31E−13	1.51E−13	...	...	...	...
NGC 4361...................	12 24 30.7	−18 47 06	1.62E−12	6.75E−14	1.07E−12	2.02E−13	−6.51E−14	0.6478	1.51	out of range	...
IC 3568	12 33 06.9	+82 33 49	5.14E−12	2.83E−13	2.96E−12	8.49E−13	5.27E−14	0.3498	1.74	out of range	...
	...	...	...	3.46E−14	...	1.04E−13	4.53E−14	...	...	...	...
NGC 5189...................	13 33 31.7	−65 58 23	3.77E−13	4.60E−14	3.00E−13	1.38E−13	−6.37E−14	0.6241	1.26	7120	—
NGC 5315...................	13 53 55.2	−66 30 52	1.08E−12	3.64E−14	1.90E−12	1.09E−13	1.06E−13	0.5320	0.57	58,500	—
PN G342.1+27.5	15 22 19.3	−23 37 31	1.06E−11	7.06E−14	7.25E−12	2.12E−13	−4.57E−14	0.4228	1.46	1170–1470	>6.9
IC 4593	16 11 44.5	+12 04 17	8.32E−13	4.29E−14	4.44E−13	1.29E−13	−1.08E−14	0.3637	1.87	out of range	...
	...	...	...	4.07E−14	...	1.22E−13	−9.61E−15	...	...	...	...
NGC 6210...................	16 44 29.5	+23 48 00	6.74E−12	5.65E−14	5.28E−12	1.69E−13	1.53E−13	0.4977	1.28	6450–6820	>3.1
	...	...	...	3.50E−14	...	1.05E−13	8.69E−14	...	...	...	...
IC 4634	17 01 33.7	−21 49 31	8.28E−13	4.42E−14	6.57E−13	1.33E−13	−3.87E−14	0.4759	1.26	7010	—
NGC 6302...................	17 13 44.4	−37 06 11	4.60E−13	3.24E−14	3.69E−13	9.72E−14	1.64E−14	0.4363	1.25	7450	—
	...	...	...	3.57E−14	...	1.07E−13	8.36E−15	...	...	...	...

TABLE 1—*Continued*

Object	R.A. (J2000.0)	Decl. (J2000.0)	F(1906.7)	1 σ error	F(1908.7)	3 σ	F(1909.6)	FWHM	F(1907)/F(1909)	N_e (cm^{-3})	$r(^{12}C/^{13}C)$
PN G345.2−08.8	17 45 35.3	−46 05 23	1.34E−12	4.07E−14	1.06E−12	1.22E−13	−7.79E−17	0.3101	1.26	6880–8240	>0.08
	. . .	. . .	. . .	5.09E−14	. . .	1.53E−13	−1.31E−14	. . .	. . .	. . .	. . .
NGC 6543	17 58 33.4	+66 38 00	9.25E−12	1.21E−13	7.38E−12	3.64E−13	−6.68E−14	0.4973	1.25	7250–7830	>1.5
	. . .	. . .	. . .	4.81E−14	. . .	1.44E−13	−1.97E−14	. . .	. . .	. . .	. . .
NGC 6572	18 12 06.4	+06 51 13	1.37E−11	1.07E−13	1.47E−11	3.20E−13	−1.46E−13	0.3302	0.93	21,900–22,200	>1.7
	. . .	. . .	. . .	2.23E−14	. . .	6.68E−14	6.38E−14	. . .	. . .	. . .	. . .
NGC 6644	18 32 34.7	−25 07 44	1.13E−11	2.60E−13	8.13E−12	7.80E−13	−4.17E−13	0.2668	1.39	3060–4080	>0.82
	. . .	. . .	. . .	4.64E−14	. . .	1.39E−13	−5.36E−14	. . .	. . .	. . .	. . .
IC 1297	19 17 22.8	−39 36 46	4.43E−12	1.12E−13	3.47E−12	3.35E−13	−2.14E−13	0.4832	1.28	6450–7580	>0.33
NGC 6818	19 43 58.3	−14 09 09	1.09E−11	2.81E−13	6.29E−12	8.42E−13	−6.23E−13	0.5499	1.73	out of range	. . .
	. . .	. . .	. . .	4.04E−14	. . .	1.21E−13	−3.31E−15	. . .	. . .	. . .	. . .
NGC 6826	19 44 48.2	+50 31 30	1.15E−11	1.34E−13	8.21E−12	4.05E−13	−3.86E−14	0.5048	1.40	2760–3280	>2.8
	. . .	. . .	. . .	9.47E−14	. . .	2.84E−13	4.56E−14	. . .	. . .	. . .	. . .
NGC 6853	19 59 36.2	+22 43 16	1.69E−12	5.09E−14	1.19E−12	1.53E−13	−6.70E−14	0.6093	1.42	2250–3580	>0.46
NGC 6891	20 15 08.9	+12 42 17	2.40E−12	3.81E−14	1.73E−12	1.14E−13	1.21E−14	0.3325	1.39	3140–3840	>1.7
	. . .	. . .	. . .	4.02E−14	. . .	1.21E−13	−3.20E−14	. . .	. . .	. . .	. . .
NGC 6905	20 22 22.9	+20 06 16	2.07E−12	6.85E−14	1.38E−12	2.06E−13	−1.46E−13	0.9453	1.50	250	—
NGC 7009	21 04 10.8	−11 21 49	1.49E−11	7.09E−14	1.22E−11	2.13E−13	1.92E−13	0.4601	1.22	8360–8570	>5.6
	. . .	. . .	. . .	9.99E−14	. . .	3.00E−13	2.34E−13	. . .	. . .	. . .	. . .
NGC 7027	21 07 01.6	+42 14 10	3.64E−12	1.39E−13	4.88E−12	4.16E−13	2.07E−13	0.3556	0.75	36,200	—
	. . .	. . .	. . .	5.90E−14	. . .	1.77E−13	1.36E−13	. . .	. . .	. . .	. . .
PN G086.5−08.8	21 33 08.0	+39 38 04	2.38E−12	4.70E−14	1.51E−12	1.41E−13	−4.04E−14	0.6668	1.58	out of range	. . .
	. . .	. . .	. . .	5.35E−14	. . .	1.61E−13	−3.49E−14	. . .	. . .	. . .	. . .
IC 5217	22 23 55.8	+50 58 00	8.79E−13	5.37E−14	6.66E−13	1.61E−13	1.01E−14	0.3017	1.32	5090	—
NGC 7662	23 25 54.0	+42 32 06	4.55E−11	2.15E−13	3.53E−11	6.44E−13	−2.49E−14	0.5772	1.29	6060–6270	>6.5
	. . .	. . .	. . .	8.78E−14	. . .	2.63E−13	4.84E−14	. . .	. . .	. . .	. . .

NOTE.—Units of right ascension are hours, minutes, and seconds, and units of declination are degrees, arcminutes, and arcseconds.

TABLE 2
EFFECTIVE COLLISION STRENGTHS AND TRANSITION PROBABILITIES FOR FOUR-LEVEL C III

| | T_e | | | | A_{ji} |
i–j	5000	10,000	15,000	20,000	(s^{-1})
1–2[a]..........................	0.13	0.11222	0.10711	0.10556	0 (for ^{12}C)
					9.04E−4 (for ^{13}C)[c]
1–3[a]..........................	0.39	0.33667	0.32133	0.31667	103[d,e]
1–4[a]..........................	0.65	0.56111	0.53556	0.52778	5.14E−3[c]
2–3[b]	0.800	0.950	1.01	1.03	2.39E−7[f]
2–4[b]	0.590	0.695	0.797	0.855	1.4E−13[c]
3–4[b]	2.23	2.75	3.05	3.23	2.39E−6[c]

[a] D. Griffin 2003, private communication, using Mitnik et al. 2003 partitioning among levels according to statistical weights.
[b] Keenan et al. 1992.
[c] Brage et al. 1998.
[d] Doerfert et al. 1997.
[e] Jönsson & Froese Fischer 1998.
[f] Fleming et al. 1996.

We also write an analogous equation for the ratio of the main lines: $I(1907)/I(1909) = I_{41}/I_{31}$ as

$$\frac{I_{41}}{I_{31}} = \frac{\nu_{41}}{\nu_{31}} \frac{(rm_4 + n_4)A_{41}}{(rm_3 + n_3)A_{31}}. \quad (12)$$

For each of the sources in Table 1, there are measured flux ratios for $F(1907)/F(1909)$. In addition, an upper limit to $F(1910)/F(1909)$ may be set by using 3 σ as the upper limit for the nondetected 1910 Å lines. (Because lines in this multiplet are so close together, intrinsic flux ratios are equivalent to observed flux ratios.)

Equations (11) and (12) are two relations that depend on r and N_e, with only a weak dependence on T_e. For the solu-

FIG. 2.—Ratio of volume emissivities vs. log (N_e cm^{-3}), from top to bottom: j_{1907}/j_{1909} for pure ^{13}C and ^{12}C, respectively, j_{1910}/j_{1909} for pure ^{13}C. Note that the j_{1909} values *differ* for the ^{12}C and ^{13}C curves. The solid and dashed lines are for $T_e = 10,000$ and 15,000 K, respectively.

tion of these equations, we use $T_e = 10,000$ K. An iterative solution converged rapidly with the results for N_e cm^{-3} and r, the ^{12}C/^{13}C abundance ratio, entered in the last two columns of Table 1. Just as rapidly, there is an indication when there is no possible solution. For these cases, a dash is shown in the ^{12}C/^{13}C column, with the N_e value found assuming pure ^{12}C. The reason that a range in N_e is shown for those PNs with a lower limit for ^{12}C/^{13}C is that the higher number for N_e corresponds to the solution of equations (11) and (12) for that limiting value of r. This value of N_e is in fact an upper limit to the actual N_e, which may range down to the smaller number shown for pure ^{12}C.

4.1. *The Flux Ratio F(1907)/F(1909)*

For some of the PNs, we found that the measured 1907/1909 Å flux ratio was higher than the theoretical low-N_e limit for ^{12}C of 1.511, 1.526, and 1.537 at T_e of 10,000, 15,000, and 20,000 K, respectively. For instance, NGC 6818 has $F(1907)/F(1909) = 1.73$, significantly higher than the atomic data predict. Rubin et al. (2001) found a similar problem for other N_e-diagnostic line ratios. In the most recent work, Rubin (2004) found that the observed [Ne v] 14.3/24.3 μm flux ratio was out of theoretical bounds on the low-N_e limit for 10 out of 20 PNs in the *Infrared Space Observatory* (*ISO*) archive, including NGC 6818.

A mixture of ^{13}C with ^{12}C helps to close the gap somewhat. The theoretical low-N_e limit for ^{13}C is 1.653, 1.658, and 1.660 at T_e of 10,000, 15,000, and 20,000 K, respectively. However, even if half the carbon were ^{13}C, observed $F(1907)/F(1909)$ ratios as high as 1.73 would not be explained. Indeed, any ratio exceeding the 5/3 value would not comport with present predictions. The value of 5/3 is the result of the standard practice of partitioning the $^1S_0$–$^3P_J^o$ multiplet value among the fine-structure levels according to the statistical weights (1, 3, 5). Consequently, this 5/3 limit does not depend on whose set of collision strengths is employed, as long as they are partitioned in this way.

An observational program to measure very accurate $F(1907)/F(1909)$ ratios would be most useful. On the theoretical side, a detailed calculation for the effective collision strengths between these individual *LS* levels would be extremely valuable.
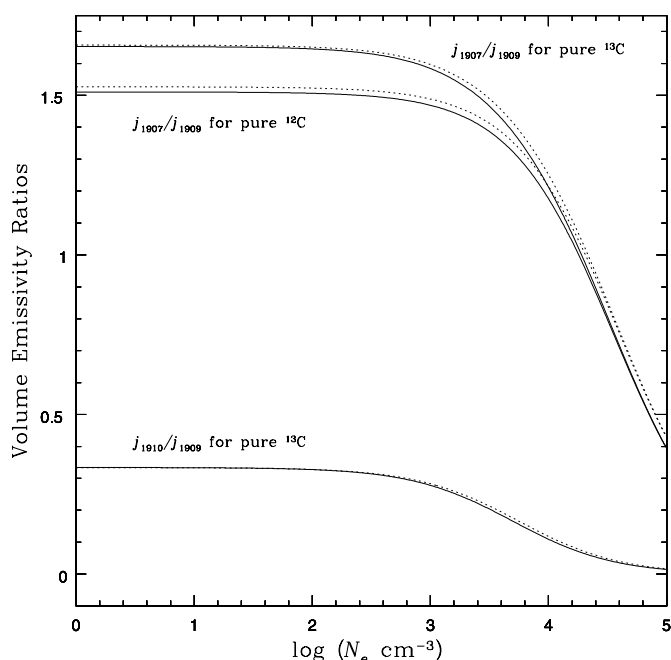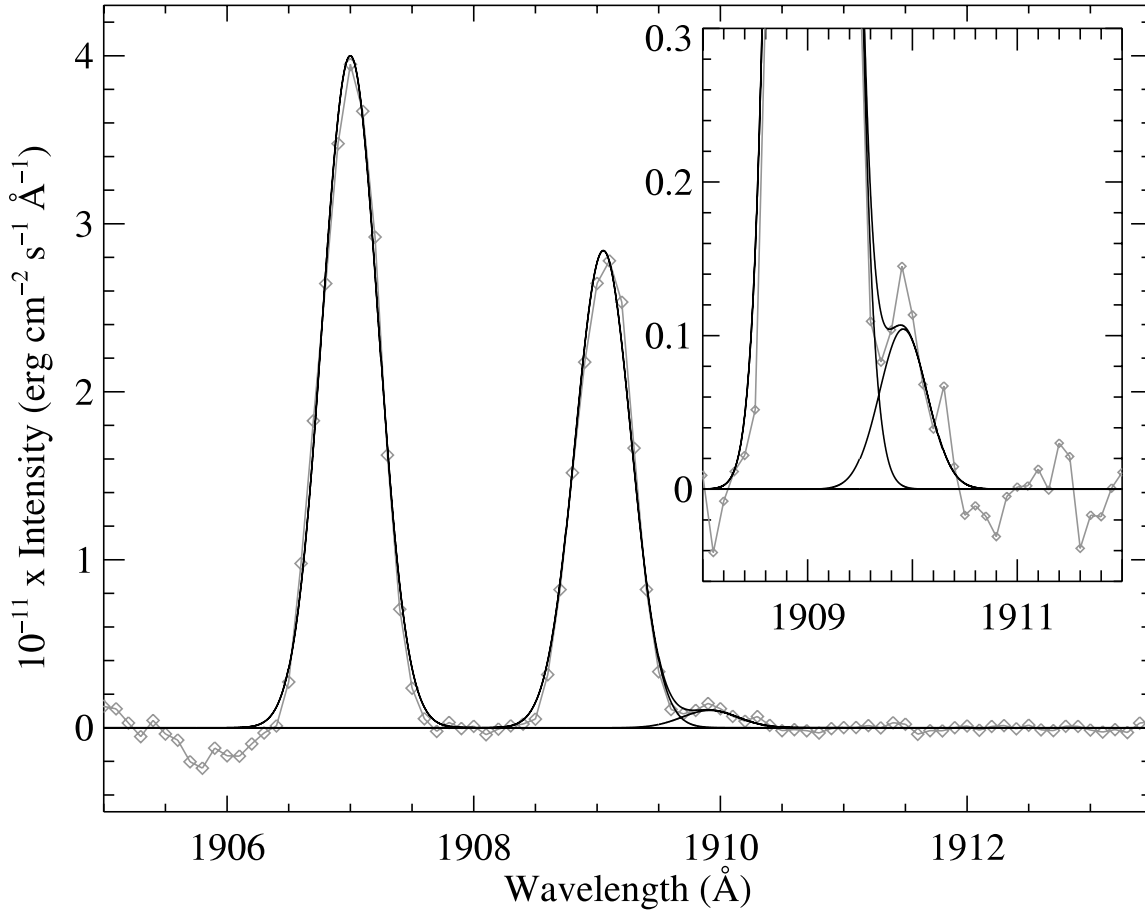
Fɪɢ. 3.—Spectrum in the vicinity of the C ɪɪɪ multiplet for NGC 2440 resulting from the co-addition of *IUE* high-dispersion, large-aperture spectra SWP 7263 and LWR 10741. The continuum is very weak compared with the 1907 and 1909 Å lines and has been fitted with a quadratic baseline and removed. The inset shows a magnified (in intensity) view of the ^{13}C 1910 Å line. The three-component Gaussian fit (see text) and sum are shown, as well as the line connecting the data points (*diamonds*).

4.2. *The Flux Ratio F(1910)/F(1909): Detection of the ^{13}C Line in NGC 2440*

The *IUE* data and analysis presented in Table 1 show only one source, NGC 2440, with a significant detection of the ^{13}C line (Fig. 3). This is the co-added spectrum of two archival spectra SWP 7263 and LWR 10741. The apertures for both spectra were centered at the same position. The position angles of the aperture major axis were 199°.19 and 20°.32, respectively (~1° mismatch), thus providing nearly the same sky coverage. Exposure times were 3600 s on 1979 November 29 and 16,200 s on 1981 May 29, respectively, and were observed under programs NCBJH and NPDJH (PI J. Patrick Harrington).

In the co-added spectrum, the observed flux of the 1909.6 Å line is $(5.94 \pm 1.47) \times 10^{-13}$ ergs cm^{-2} s^{-1}, which is a 4 σ detection. The simultaneous solution of equations (11) and (12), assuming $T_e = 10{,}000$ K, gives $N_e = 2460$ cm^{-3} and ^{12}C/^{13}C = 4.4. With an assumed T_e of 15,000 K, the solution becomes $N_e = 3130$ cm^{-3} and ^{12}C/^{13}C = 4.2. We prefer the former solution because according to Figure 2 (T_e vs. ionization potential [IP]) in Bernard Salas et al. (2002), it appears that the T_e value for the C^{++} zone in NGC 2440 is closer to 10,000 than 15,000 K for the case C$^+$ → C^{++} with IP 24.4 eV. Although not sensitive to the assumed T_e, the general trend we find here is that the higher the T_e, the higher the derived N_e and the lower the derived ^{12}C/^{13}C. We estimate the uncertainty

in the value of ^{12}C/^{13}C as ± 1.2 from separate measurements and analysis of the two individual *IUE* spectra.

In their study of NGC 2440, Bernard Salas et al. (2002) used these same two *IUE* spectra. According to their Table 3, $F(1907) = 2.43 \times 10^{-11}$ and $F(1909) = 1.77 \times 10^{-11}$ ergs cm^{-2} s^{-1}. This leads to $F(1907)/F(1909) = 1.373$, while they have a slightly different ratio of 1.35 in their Table 5, where they also list the derived $N_e = 4360$ cm^{-3}, assuming $T_e = 15{,}000$ K. We compare these to our entries in Table 1: $F(1907) = 2.24 \times 10^{-11}$ and $F(1909) = 1.57 \times 10^{-11}$ ergs cm^{-2} s^{-1}. This leads to $F(1907)/F(1909) = 1.427$, which results in a lower derived N_e, irrespective of accounting for the effect of the presence of ^{13}C. It is not clear why their line fluxes are higher than ours. It may be due to several factors. For instance, they may have used the pre-NEWSIPS calibration. They likely used a different technique than ours to form a weighted average of the two *IUE* spectra. Their fluxes might be taken directly from the Gaussian-fit areas, whereas we have used Gaussian fits for guidance but use the option in ISAP (*moment* fit) and IRAF (*splot* "e" option) to measure the areas (except for measuring the 1910 Å line with the Gaussian). Generally we find that departures from a Gaussian profile result in somewhat smaller line fluxes. Additionally, the fitting of lines is not totally objective, e.g., in the manner of accounting for the baseline.

Although the line was not detected in any of the other PNs, we were able to establish lower limits for the ^{12}C/^{13}C ratio for

many. Even when co-adding many spectra, the S/N was not high enough to ascertain a useful value of ^{12}C/^{13}C for most objects. *HST* studies similar to those of Palla et al. (2002) and Clegg et al. (1997) could be used to refine the limits presented here.

At a late stage in our work on this project, we were surprised to discover that a similar project had been undertaken by Miskey, Feibelman, & Bruhweiler (2000). They report a detection in NGC 2440, but appear to derive a much higher ^{12}C/^{13}C ratio of 39. They also report a detection in NGC 6302 with a ratio of 23. Unfortunately, since only an AAS abstract has been published, their data and methods are not available for scrutiny. We cannot report a detection of the 1910 Å line in NGC 6302. Two short-wavelength spectra (SWP 10391 and SWP 8971) and one long-wavelength spectrum (LWR 7722) are available for this nebula. Even the 1907, 1909 main lines are indistinguishable from the noise in LWR 7722; co-adding SWP 10391 and SWP 8971 produces a nondetection of the 1910 Å line. SWP 10391 shows a small peak at the correct location, but at the same level as the noise; thus, a detection cannot be conclusively claimed.

While 10 SWP and eight LWP/LWR spectra were available for NGC 3918, many of them showed saturation in the strong C III lines, making them unusable for determining ratios. Similarly, all four available SWP spectra for NGC 3242 are saturated, and the values from Table 1 come from only LWR 12705. Our limits are consistent with the findings of Clegg et al. (1997) and Palla et al. (2002). We note that Palla et al. used a 1 σ upper limit for $F(1910)$, while we use 3 σ. Using their 1 σ value and main-line fluxes for NGC 3242 with our improved atomic data here, we find that their ^{12}C/^{13}C $\geq$ 38 becomes $\geq$44.4. However, when we use a 3 σ observed upper limit from their paper, then more conservatively ^{12}C/^{13}C $\geq$ 14, a value very similar to our limit in Table 1.

5. DISCUSSION AND CONCLUSIONS

NGC 2440 has an unusually massive central star (CS), of mass 0.72 $M_{\odot}$, according to Wolff, Code, & Groth (2000), or 0.932 $M_{\odot}$, according to Górny, Stasińska, & Tylenda (1997). The progenitor star is believed to be more massive than 4 $M_{\odot}$; e.g., Figure 3 in Balser et al. (2002) has $\sim$4.2–4.3 $M_{\odot}$ (see also the discussion in their § 2). In their study of NGC 2440, Bernard Salas et al. (2002) concluded, based on a measured (C+N+O)/H ratio higher than that for NGC 7027, that the CS must have been a more massive progenitor than was the star in NGC 7027, for which Bernard Salas et al. (2001) found 3–4 $M_{\odot}$. Above 4 $M_{\odot}$, asymptotic giant branch (AGB) stars develop deep convective envelopes with very high base temperatures, leading to the operation of the CN cycle; hence the name, hot-bottom burning. There, the CN cycle operates at the base of the convective envelope in a hydrogen-burning shell, where ^{12}C is converted into ^{13}C and then into ^{14}N. This process would tend to drive ^{12}C/^{13}C toward the CN cycle equilibrium ratio of $\sim$3.3 (Smith & Lambert 1990; Frost et al. 1998). When ratios close to the CN cycle equilibrium value are measured in a star's atmosphere, it is indicative of the presence of nearly pure CN cycle material. Thus, the low ^{12}C/^{13}C ratio of 4.4 $\pm$ 1.2 that we find for NGC 2440 does support this picture.

If the progenitor were less massive than 4 $M_{\odot}$, then the scenario changes. Both the cool-bottom processing (CBP) and standard models predict ^{12}C/^{13}C $\simeq$ 20–30 for stars between 3 and 4 $M_{\odot}$ (Boothroyd & Sackmann 1999; Renzini & Voli

1981). Then our derived ^{12}C/^{13}C for NGC 2440 would not appear to support either the standard or CBP theories. While CBP does produce ratios as low as 4.4, it is only expected to occur in progenitor stars of $\leq$2 $M_{\odot}$ (Wasserburg, Boothroyd, & Sackmann 1995). Two (unlikely) possibilities might allow agreement. First, were the mass estimates for the CS progenitor too large by a factor of $\sim$2, our ^{12}C/^{13}C = 4.4 for NGC 2440 would support the CBP theory. Second, perhaps CBP occurs in stars of 3–4 $M_{\odot}$. This is, in fact, contrary to the statement by Wasserburg et al. (1995) that no CBP is expected above $\sim$2.3 $M_{\odot}$. However, a reconsideration of model parameters might be useful for determining whether this could occur.

The small ^{12}C/^{13}C we find for NGC 2440 is in the range derived by Balser et al. (2002) in their study of molecular clouds associated with PNs. As mentioned in § 1, from observations of ^{12}CO and ^{13}CO millimeter lines, they found values of ^{12}C/^{13}C from 2.2 to 31 in nine PNs. The lowest value 2.2 $\pm$ 0.03 was for the bipolar PN M1-16, which is not on our list. We note that our small ratio for NGC 2440 is consistent with measurements of J-type carbon stars. Abia & Isern (1997) found $\langle^{12}$C/^{13}C$\rangle$ = 6 $\pm$ 3, while Ohnaka & Tsuji (1999) in their analysis of 26 J-type C stars found an even lower average of 4.7 $\pm$ 2.8, with several ratios as low as $\sim$1–2, well below the equilibrium value for the CN cycle.

The question remains as to why NGC 2440 is the only nebula among those we measured that has a detectable 1909.6 Å ^{13}C hyperfine structure line, as well as why it has such a low ^{12}C/^{13}C. Using *IUE* archival data, we also set upper limits on $F(1909.6)$ in 40 other PNs available and lower limits for ^{12}C/^{13}C in 23 of these. *IUE* had limited dynamic range that precludes setting more stringent limits for most objects, though co-adding spectra allows better S/N. NGC 2440 is among the brightest PNs in terms of either of the main-line fluxes; only NGC 2867, NGC 3242, NGC 3918, and NGC 7662 are higher (see Table 1). By using the measured 3 σ as an upper limit to their $F(1909.6)$, we derive lower limits on ^{12}C/^{13}C for these four nebulae of, respectively, 5.9, 14.5, 9.9, and 6.5—already higher than what we find for NGC 2440. NGC 2440 is carbon-rich, with C/O of 1.9 (Bernard Salas et al. 2002), and a high-excitation Peimbert type I PN (Hyung & Aller 1998); that is, it is an N- and He-rich PN. The central star is among the hottest ($\sim$200,000 K) and most massive known (see above). In fact, in their entire sample of $\sim$80 PNs, Górny et al. (1997) derived a CS mass of 0.932 $M_{\odot}$, which was the second largest of all. This nebula also has T_e reaching as high as 15,000–20,000 K, as measured in several high-ionization species (Bernard Salas et al. 2002). NGC 2440 has a relatively low N_e of 2460 cm^{-3} determined here (see Table 1). Both lower N_e and lower ^{12}C/^{13}C lead to a higher $F(1910)/F(1909)$. It may be that type I PNs have lower ^{12}C/^{13}C ratios. Furthermore, NGC 2440 is a bipolar PN. In their study, Balser et al. (2002) found that those PNs that have the lowest values of ^{12}C/^{13}C are classified as bipolar. Further theoretical and observational work is needed to determine the cause of the low ratios. An *HST* spectroscopic study of the C III multiplet in NGC 2440 would be desirable.

Several of the PNs have the measured $F(1907)/F(1909)$ outside the low-N_e theoretical limit for ^{12}C. Uncertainties in the measured fluxes may account for some of these differences. A mixture of ^{13}C with ^{12}C helps narrow the gap somewhat. Nevertheless, some of the observed $F(1907)/F(1909)$ ratios still appear too high to conform to the currently

predicted limits. We have shown that both the $F(1907)/F(1909)$ and the $F(1910)/F(1909)$ ratios in the low-N_e limit are predominantly influenced by using the standard partitioning among the collision strengths for the multiplet $^1S_0-^3P_J^o$, according to the statistical weights. A detailed calculation for the effective collision strengths between these individual levels would be valuable. The determination of reliable N_e values by this method as well as the $^{12}C/^{13}C$ abundance ratio depends on it. As far as we know, it appears that there have been no previous attempts to account for the presence and effects of ^{13}C when using the well-known C III N_e diagnostic $F(1907)/F(1909)$.

REFERENCES

Abia, C., & Isern, J. 1997, MNRAS, 289, L11

Balser, D. S., McMullin, J. P., & Wilson, T. L. 2002, ApJ, 572, 326

Bernard Salas, J. B., Pottasch, S. R., Beintema, D. A., & Wesselius, P. R. 2001, A&A, 367, 949

Bernard Salas, J. B., Pottasch, S. R., Feibelman, W. A., & Wesselius, P. R. 2002, A&A, 387, 301

Boothroyd, A. I., & Sackmann, I.-J. 1999, ApJ, 510, 232

Brage, T., Judge, P. G., Aboussaid, A., Godefroid, M. R., Joensson, P., Ynnerman, A., Fischer, C. F., & Leckrone, D. S. 1998, ApJ, 500, 507

Charbonnel, C., & do Nascimento, J. D. 1998, A&A, 336, 915

Clegg, R. E. S. 1985, in ESO Workshop on Production and Distribution of C, N, O Elements, ed. I. J. Danziger, F. Matteucci, & K. Kjär (Garching: ESO), 261

Clegg, R. E. S., Storey, P. J., Walsh, J. R., & Neale, L. 1997, MNRAS, 284, 348

Doerfert, J., Träbert, E., Wolf, A., Schwalm, D., & Uwira, O. 1997, Phys. Rev. Lett., 78, 4355

Fleming, J., Bell, K. L., Hibbert, A., Vaeck, N., & Godefroid, M. R. 1996, MNRAS, 279, 1289

Frost, C. A., Cannon, R. C., Lattanzio, J. C., Wood, P. R., & Forestini, M. 1998, A&A, 332, L17

Górny, S. K., Stasińska, G., & Tylenda, R. 1997, A&A, 318, 256

Hyung, S., & Aller, L. H. 1998, PASP, 110, 466

Jönsson, P., & Froese Fischer, C. 1998, Phys. Rev. A, 57, 4967

Keenan, F. P., Feibelman, W. A., & Berrington, K. A. 1992, ApJ, 389, 443

Miskey, C. L., Feibelman, W. A., & Bruhweiler, F. C. 2000, BAAS, 196, 43.04

Mitnik, D. M., Griffin, D. C., Ballance, C. P., & Badnell, N. R. 2003, J. Phys. B, 36, 717

Ohnaka, K., & Tsuji, T. 1999, A&A, 345, 233

Palla, F., Bachiller, R., Stanghellini, L., Tosi, M., & Galli, D. 2000, A&A, 355, 69

Palla, F., Galli, D., Marconi, A., Stanghellini, L., & Tosi, M. 2002, ApJ, 568, L57

Renzini, A., & Voli, M. 1981, A&A, 94, 175

Rubin, R. H. 1986, ApJ, 309, 334

———. 2004, in IAU Symp. 217, Recycling Intergalactic and Interstellar Matter, ed. P.-A. Duc, J. Braine, & E. Brinks (San Francisco: ASP), in press (astro-ph/0402447)

Rubin, R. H., Dufour, R. J., Geballe, T. R., Colgan, S. W. J., Harrington, J. P., Lord, S. D., Liao, A. L., & Levine, D. A. 2001, in ASP Conf. Ser. 247, Spectroscopic Challenges of Photoionized Plasmas, ed. G. J. Ferland & D. W. Savin (San Francisco: ASP), 479

Sackmann, I.-J., & Boothroyd, A. I. 1999, ApJ, 510, 217

Smith, V. V., & Lambert, D. L. 1990, ApJS, 72, 387

Wasserburg, G. J., Boothroyd, A. I., & Sackmann, I.-J. 1995, ApJ, 447, L37

Wolff, M. J., Code, A. D., & Groth, E. J. 2000, AJ, 119, 302